Methanol from solid fuels: A cost-effective route to reduced emissions and enhanced energy security

Carlos Arnaiz del Pozo [a], Ángel Jiménez Álvaro [a], Schalk Cloete [b,*]

[a] *Universidad Politécnica de Madrid, Spain*
[b] *SINTEF Industry, Norway*

ARTICLE INFO

ABSTRACT

Methanol (MeOH) is gaining increasing relevance as a future energy carrier. It can be produced through multiple avenues, including locally available solid fuels where the CO$_2$ footprint of coal-derived MeOH can be strongly reduced through co-gasification with biomass and integration of CO$_2$ capture and storage. This work presents a techno-economic assessment of five MeOH production processes from a 70/30 %w. coal/biomass blend under consistent cost assumptions of 2.5 €/GJ coal, 100 €/ton (6.1 €/GJ) biomass, 100 €/ton CO$_2$ tax and 60 €/MWh carbon-free electricity. The reference plant configuration reached a levelized cost of MeOH (LCOM) of 285.5 €/ton, while the two advanced concepts with a more efficient gasification system reached costs of 245.0–255.0 €/ton. Two additional cases synergistically integrating PEM electrolysers to deliver H$_2$ for improving the syngas H/C ratio and O$_2$ for gasification reached higher LCOM of 363.0–448.8 €/ton due to the higher cost contribution of electricity. An unrealistically low price of 25.6–34.7 €/MWh for a steady-state supply of carbon-free electricity is required for these configurations to break even with the benchmark plant. Finally, MeOH from the best per-forming plant was shown to be cost-competitive with gasoline produced from 60 €/barrel oil, while total CO$_2$ emissions (including combustion) were 56 % lower. Thus, MeOH from solid fuels offers a cost-effective solution to climate change and energy security in energy importing regions.

1. Introduction

Stringent climate change mitigation targets will require a rapid, economy-wide decarbonization effort [1]. The electricity sector presents the most straightforward decarbonization opportunities, but it accounts for only 20 % of global final energy consumption [2]. Hence, a wide range of solutions will be required in other sectors where hydrocarbon fuels currently dominate. To date, decarbonization strategies in these sectors have focussed on efficiency, switching to lower carbon intensity fuels such as natural gas and hydrogen, as well as electrification via renewable (solar and wind) power. Nonetheless, the use of carbon-intensive solid fuels (coal, biomass, waste) presents several advantages, as cheap locally available resources avoid the energy security risks of natural gas and the intermittency challenge of wind and solar.

A promising pathway for exploiting these benefits related to solid fuels is the production of lower-carbon fuels via energy conversion processes incorporating CO$_2$ capture and storage (CCS). Hydrogen is the most investigated alternative, but its low energy density and high flammability present substantial techno-economic challenges related to storage and distribution. Hence, alternative lower-carbon fuels are being investigated to address these practical challenges. Methanol (MeOH) is one such alternative with a range of existing industrial applications [3] and considerable potential for future deployment as a transportation fuel [4]. Although the carbon atom is preserved, potentially leading to CO$_2$ emissions upon use, it is 30 % less carbon intensive than coal, and its liquid state under ambient conditions greatly simplifies handling, storage, and transportation compared to hydrogen or other gaseous fuels.

Globally, natural gas remains the leading feedstock for MeOH production, but coal offers an economically competitive pathway with potential for CO$_2$ emissions curtailment [8]. Given that coal gasification yields syngas with a high CO/H$_2$ ratio [9], conventional coal to MeOH (CtM) technologies adjust the syngas composition through partial water gas shift (WGS) and CO$_2$ removal by absorption processes to reach a feed gas stoichiometry for chemical synthesis (Eq. (1)). Hence, CO$_2$ capture is an inherent requirement in the process.

$$M = \frac{[H_2] - [CO_2]}{[CO] + [CO_2]} \approx 2 \tag{1}$$

---

* Corresponding author at: Flow Technology Group, SINTEF Industry, S.P. Andersens vei 15B, 7031 Trondheim, Norway.
  E-mail address: schalk.cloete@sintef.no (S. Cloete).

Nomenclature

ACF	Annualized cash flows
AEM	Anion exchange membrane
ATR	Autothermal reformer
ASME	American Society of Mechanical Engineers
ASU	Air Separation Unit
BEC	Bare erected cost
BtM	Biomass to methanol
BWR	Boiling water reactor
CAPE	Computer-aided process engineering
CCS	Carbon capture & storage
CGE	Cold gas efficiency
CtM	Coal to methanol
DAC	Direct air capture
EPC	Engineering, procurement and construction
FOM	Fixed operating & maintenance costs
GE	General Electric
GHG	Greenhouse gas
GSR	Gas switching reforming
HTER	Heat transfer exchanger reformer
HTS	High temperature shift
LCOM	Levelized cost of methanol
LCOP	Levelized cost of product
LHV	Lower heating value
MDEA	Methyl di-ethanol amine
NET	Negative emissions technology
NPV	Net present value
OC	Owners costs
PC	Process contingency
PEM	Proton exchange membrane
PFSA	Perfluorosulfonic acid
PT	Project contingency
PtX	Power to X
RE	Renewable energy
RES	Renewable energy sources
SEA	Standardized economic assessment
SOEC	Solid oxide water electrolysis
TOC	Total overnight cost
T&S	Transport & storage
tpd	Tons per day
VOM	Variable operating & maintenance cost
WGS	Water gas shift

List of Symbols

M	Syngas module
η	Thermal efficiency
ϕ	Capacity factor
ε	Molar efficiency
i	Discount rate
n	Plant lifetime
t	Year
α	Charge transfer coefficient
δ	PEM relative thickness change
λ	PEM hydration ratio
σ	PEM electric conductivity ($\Omega^{-1} \cdot cm^{-1}$)
ν_i	Stoichiometric coefficient of referred substance
a_i	Activity of referred substance
$\epsilon_{AC/DC}$	AC/DC converter efficiency
A	PEM electrode surface area (cm^2)
ASR	Area-specific resistance ($\Omega \cdot cm^2$)
C_i	Annualized capital or operation cost
C_{CO_2}	Specific capture
E_{act}	Activation energy (kJ/mol)
E_{CO_2}	Specific emissions
f_P	H_2 permeability pressure enhancing factor (bar/(A/cm^2))
F	Faraday constant (C/mol)
ΔH°	Change of standard enthalpy (kJ/mol)j, Current density (A/cm^2)
j_0	Exchange current density (A/cm^2)
K_P	Permeability coefficient ((mA/cm^2)·(μm/bar))
L_0	PEM dry thickness (μm)
L	PEM actual thickness (μm)
P_{MeOH}	Yearly MeOH production
ΔS°	Change of standard entropy (J/(mol·K))
SC	Specific consumption (GJ/ton)
$\dot{m}$	Mass flow (kg/s)
n_d	Electro-osmotic dragg coefficient
n_e	Number of transferred electrons per reactant molecule
$\dot{n}$	Molar flow (mol/s)
$\dot{n}_P$	Molar permeation rate (mol/s)
P	Pressure (bar)
P_i	Partial pressure of referred substance (bar)
P^v	Water vapour pressure (bar)
R	Ideal gas constant (J/(mol·K))
T	Thermodynamic temperature (K)
$T(^\circ C)$	Temperature in Celsius degrees
V	Voltage (V)
w	Specific electric energy consumption (kJ/mol)
$\dot{W}$	Power (kW)

The competitiveness of CtM processes can be further improved by minimizing the primary energy consumption. For example, the development and deployment of advanced process units like chemical looping air separation and chemical looping hydrogen production ([10,11]) or the integration of coal gasification and coking [12] can improve economic performance and reduce emissions. Furthermore, two-stage gasification systems with slurry vaporization ([13,14]) and advanced syngas treating units such as hot gas clean up (HGCU) [15] achieve considerable efficiency improvements relative to one stage gasifiers with costly heat management options such as radiant syngas coolers and low temperature contaminant removal. Cheaper options such as full water quench are available, at the cost of decreased electricity generation [16].

An alternative pathway to satisfying the stoichiometric requirements for MeOH production (Eq. (1)) is to add additional hydrogen instead of removing excess CO_2. This pathway presents an interesting synergy between MeOH production from solid fuels and electrolysis powered by renewable energy sources (RES) like wind and solar [17]. If the required quantity of electrolytic hydrogen is supplied, syngas shift and CO_2 removal units can be avoided while the O_2 by-product from the electrolyser can be utilized as oxidizing agent in the gasifier, eliminating the costly air separation unit (ASU). Since carbon efficiency is enhanced though the avoidance of CO_2 removal, the solid fuel heat input decreases for a fixed MeOH production rate, lowering the number of costly gasifier units and associated plant scope. Getting the carbon atom from solid fuels in such a hybrid configuration may be more economical than sourcing it from CO_2 as required for green MeOH production from electrolytic hydrogen, which is projected to remain twice as costly as conventional methods by 2050 [7]. In accordance, Su et al. [18] found that direct CO_2 hydrogenation plants through RES are economically unfeasible without favourable subsidy policies.

Another important consideration in MeOH production from solid

fuels is the potential of biomass to reduce the total greenhouse gas emissions of the product. For example, biomass to methanol (BtM) achieves a net negative global warming potential when considering the full lifecycle of MeOH production, a large improvement over the conventional CtM route [19]. However, sustainably produced biomass is a limited resource, and coal-biomass blending may therefore be necessary to prevent the environmental impacts of overexploitation. With a

suitable increase in CO_2 taxation, MeOH from a blend of torrefied biomass and coal can outperform the conventional CtM process [20]. Coal-biomass blending can also enable high temperature gasification that minimizes tar formation, although the maximum biomass fraction must be limited to prevent aggressive ash from damaging the refractory lining of the gasifier [21]. However, larger biomass fractions reduce MeOH yield [22].
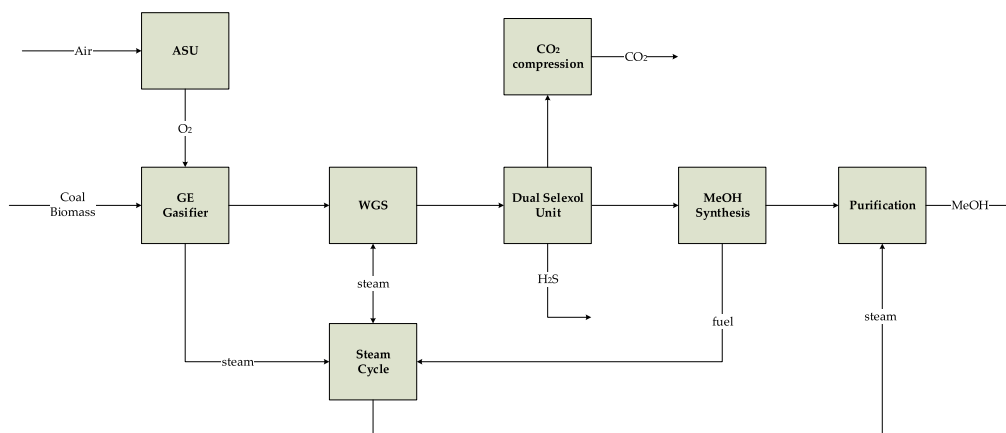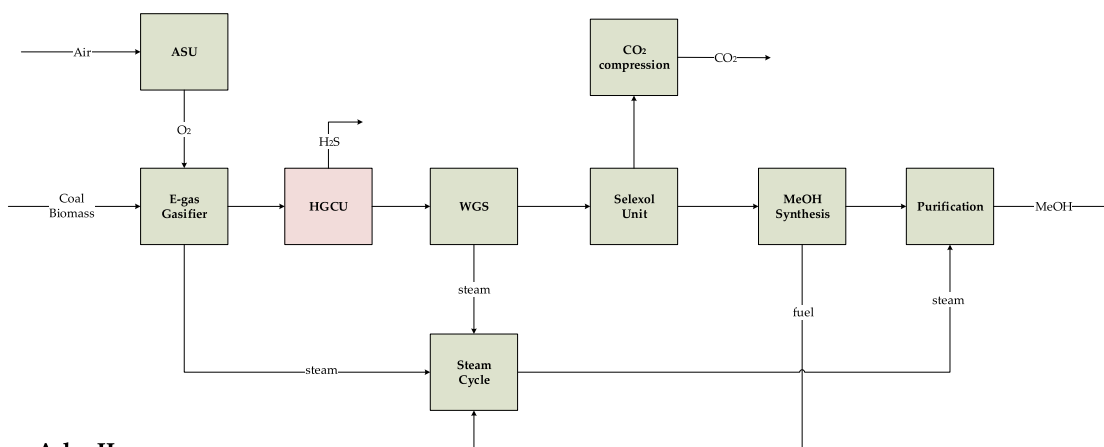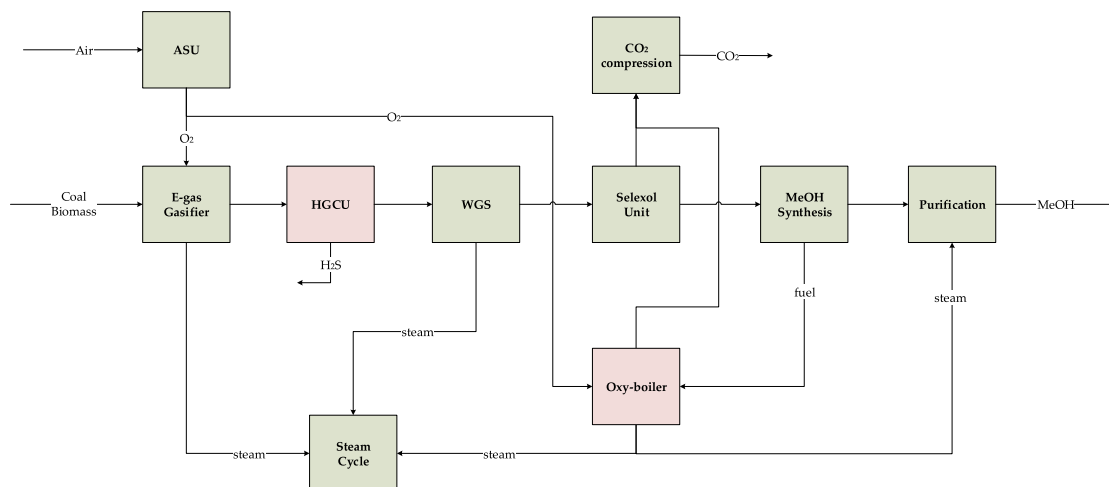

Fig. 1. Block flow diagram of MeOH plants from solid fuels.

Combining biomass gasification with electrolysis [23] can also improve environmental performance while limiting biomass consumption. In addition, electrolytic hydrogen production opens the potential for flexible operation to integrate higher shares of wind and solar power. However, high capacity factors are required to minimize costs [23], indicating that flexibility should be exploited to avoid electricity price peaks and not to capitalize on limited periods of excess electricity. These concepts would benefit from potential capital cost reductions of the electrolyser, which is essential for the competitiveness of biomass-electrolysis hybrid MeOH plants [24].

Building upon this broad range of possibilities for low-carbon MeOH production from solid fuels, the contribution of the present work is twofold: 1) compare multiple process layouts using a standardized techno-economic methodology and 2) benchmark selected solid fuel configurations against MeOH production from other feedstocks. Recognizing the importance of efficiency gains and the potential to integrate biomass and electrolytic hydrogen, a techno-economic assessment of five MeOH plant configurations from coal-biomass blends is carried out, incorporating advanced gasification systems and syngas treating technologies, as well as alternative H_2 supply through PEM electrolysers. The levelized cost of MeOH (LCOM) is calculated through a detailed bottom-up economic assessment and sensitivity studies to key economic assumptions are performed for each case. Subsequently, the LCOM of selected configurations is benchmarked against regular gasoline and alternative MeOH production pathways

from natural gas and renewables assessed using the same methodology [7]. Such a holistic comparison allows clear conclusions to be drawn regarding the potential of MeOH from solid fuels as a secure and low-carbon fuel for the future.

1.1. Technology overview

The main features of the MeOH plants from solid fuels assessed in this work are succinctly detailed in this section with detailed flow diagrams and stream summaries available in the Supplementary Material. Three plants utilize only a coal-biomass blend (Ref., Adv. I and Adv. II) and are depicted in Fig. 1, while two combine solid fuels and renewable power as primary energy feedstocks (El. I and El. II), shown in Fig. 2:

- **Ref.**: The reference MeOH plant consists of a GE gasifier with radiant cooler, quench and syngas scrubbing, producing a syngas with a high CO/CO_2 ratio, followed by a partial shift and dual selective CO_2 and H_2S removal to adjust the syngas module prior to the synthesis loop.
- **Adv. I**: The advanced MeOH plant utilizes a two stage E-gas gasifier with slurry vaporization (thereby improving the cold gas efficiency (CGE) relative to the reference plant) and HGCU for H_2S removal. A simplified Selexol unit removes sufficient CO_2 to adjust the syngas composition for the synthesis loop.
- **Adv. II**: This enhanced configuration employs higher purity O_2 from the ASU to achieve a lower inert concentration in the synthesis loop,
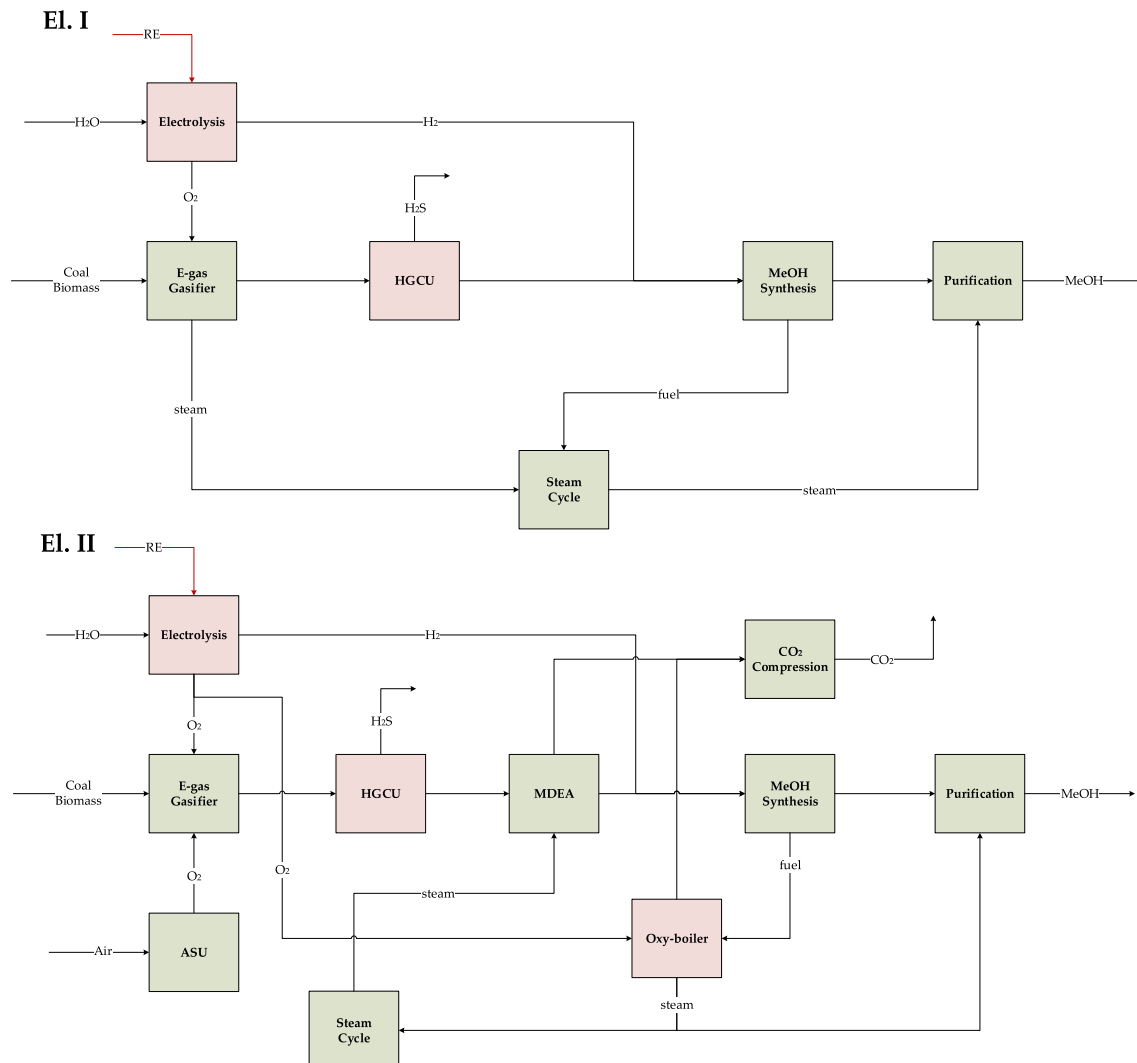

Fig. 2. Block flow diagram of MeOH plants from solid fuels and renewable energy (RE).

routing the purge steam to an oxy-boiler, to attain almost complete CO_2 capture.

- **El. I**: This concept incorporates the advanced E-gas gasifier and HGCU while supplying a large portion of the H_2 through water electrolysis, thus reducing the solid fuel heat intake for a fixed MeOH production. Furthermore, an ASU is not required as the electrolyser generates sufficient O_2 as by-product to carry out the gasification process. This configuration is attractively simple, avoiding the need of a partial syngas shift and CO_2 removal from the syngas (and thus compression and storage requirements).

- **El. II**: This configuration includes additional scope for CO_2 removal with MDEA to significantly reduce the H_2 production demand from the electrolyser unit to achieve a stoichiometric syngas feed gas for synthesis. On top of that, the purge stream from the synthesis loop is combusted in an oxy-boiler, thereby practically eliminating CO_2 emissions relative to the El. I case. A small ASU is still required as the electrolyzer does not produce sufficient O_2.

The time-horizon envisaged for the deployment of the concepts discussed is 2050, and several technological advances are required in the interim for successful commercialization, with differing degrees of criticality. Specifically, the development of advanced gasification systems with a high cold gas efficiency and operational reliability is of high importance to attain attractive foreseen gains [13], while substantial scale-up and cost reductions of electrolyser technology is essential for the feasibility of the last two concepts. To a lesser extent, de-risking of high temperature syngas clean-up and oxy-combustion boilers enable lower capital investment and increased CO_2 emissions mitigation,

respectively, but unforeseen challenges could be circumvented at a mild penalty using conventional technologies.

2. Methodology

The techno-economic assessments carried out in the present study follow the same approach as that discussed in earlier work [7], where stationary plant models of different configurations are developed, followed by a bottom-up economic analysis. Fig. 3 shows an outline of the methodology employed for the evaluation. The Peng-Robinson [25] equation of state (EoS) was specified for thermodynamic property estimation of streams containing air or light hydrocarbons, while ASME steam tables were selected for the power cycle. All configurations employ the same purification unit and MeOH synthesis loop, with a boiling water reactor (BWR) modelled using kinetics for CO_2 hydrogenation and reverse WGS reactions from Bussche et al. [26] operated at 230 °C and 75 bar, within the typical range found in industrial applications [6]. The gasification and syngas treating units are presented in greater detail in an earlier study [14]. On the other hand, a dedicated model for the electrolyser was developed in Scilab, based on the parameters reflected in Falcão et al. [17] and Rivera-Tonoco et al. [17,27], and presented in a subsequent section. The electrolyser was sized according to the H_2 requirements of each plant, thus determining the electricity consumption. Anode and cathode stream outlets were transferred to the stationary plant model in Unisim Design R481 by means of a CAPE-OPEN unit operation.

In this section further technical details of the reference, advanced and blue-green electrolyser MeOH production plants from solid fuels are
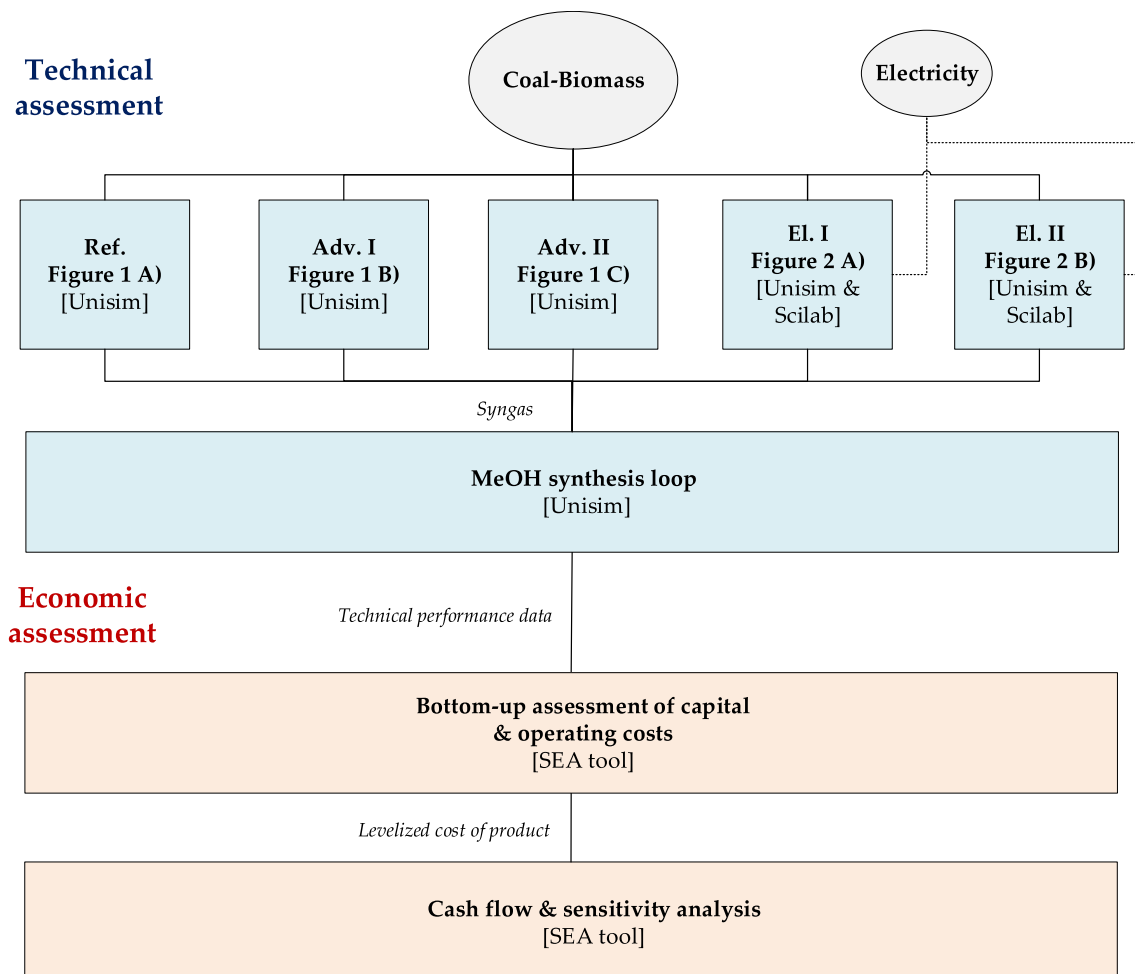

Fig. 3. Methodology and tools employed in the techno-economic assessment.

provided. The plants are designed for a baseline production capacity of 10,000 tpd, employing a blend of Douglas Premium coal [28] and woody biomass [29] with a 30 %w. fraction of the latter. Plants Ref., Adv. I and Adv. II are designed consisting of four parallel gasifiers with an approximate heat input of 1000 MW each [30], while the ASUs and syngas treating units are designed as two parallel trains, to supply syngas to the synthesis loop. On the other hand, the cases with electrolyser (El. I & El. II) consist of two parallel gasifiers and one syngas treating train, reflecting the scope reduction potential of this technology integration at an equivalent MeOH production rate.

2.1. Reference MeOH plant

The reference MeOH production plant features a slurry-fed GE gasifier operating at 1350 °C and 80 bar with a radiant syngas cooler to cool down the syngas, producing superheated high pressure steam [30]. O_2 with a 95 %mol purity is delivered by a low pressure, pumped liquid oxygen air separation unit (ASU), suitable for high pressure gasifier operation which results in reduced syngas compression requirements prior to the synthesis loop, and enables the use of a physical sorbent in the CO_2 removal unit downstream since the partial pressure of this component is sufficiently high. The syngas is further cooled through a water quench prior to a syngas scrubbing step, modelled with as a three-stage equilibrium column. The scrubber bottoms stream is cooled down by preheating the 65 %w. slurry feed to 200 °C. The syngas product after scrubbing is at around 250 °C and has a large amount of water (~60 % mol). A fraction of this stream shifted at high temperature in an adiabatic WGS reactor to attain a suitable MeOH synthesis composition after CO_2 removal. The reactor was modelled assuming an equilibrium conversion, similarly to Anantharaman et al. [28]. The reactor effluent and the syngas portion which is not shifted are cooled down in a heat recovery network to deliver hot water to the scrubber, gasifier quench and MeOH reactor, as well as generating LP steam to satisfy both H_2S scrubber and MeOH purification column heat demand. The syngas product at ambient temperature is subsequently routed to a dual Selexol CO_2 removal unit [31], selectively removing H_2S and CO_2 contaminants. CO_2 is compressed in a 5-stage intercooled compressor and pumped to a supercritical pressure of 150 bar, while H_2S is sent to the Claus unit, not modelled in this work but accounted for in the subsequent economic assessment. The CO_2 lean syngas product is then routed to the synthesis loop after a small booster compressor stage.

2.2. Advanced MeOH plants

Two advanced configurations are evaluated. Both plants employ a two-stage E-gas gasifier [13,32]. The first stage operates at 1350 °C and 80 bar gasifying approximately 80 % of the pre-vaporized slurry with 95 %mol pure O_2 from an ASU. The 1st stage hot outlet gases are mixed with the remaining 20 % of the feed, gasifying that portion through a chemical quench, while the solid char falls to the bottom of the gasifier. The 2nd stage outlet gases at 950 °C are cooled down by indirectly preheating and vaporizing the slurry feed thereby attaining a high cold gas efficiency and low oxygen consumption relative to the reference plant gasifier. Modifications to the original E-gas concept design are suggested Gräbner et al. [13] to enable higher pressure operation and slurry drying through direct contact with the 2nd stage gasifier outlet gases, based on the patents developed by Douglas et al. [33] and Breton et al. [34], respectively. Tars are removed with a filter from the syngas product and recycled to the 1st stage, while the syngas is routed to a hot gas desulphurization unit operating at 450 °C [15]. This syngas treating technology consists of two interconnected fluidized beds utilizing ZnO as adsorbent and can achieve promising cost and energy savings if commercialized and deployed [35,36]. Sulphur concentrations in the syngas product must be below 100 ppbv for safe MeOH catalyst operation [8], therefore a non-regenerable H_2S polishing bed might be required downstream to meet the specifications [37]. Other sorbents are

used in this unit to remove harmful contaminants such as chlorides and ammonia from the syngas [38]. N_2 from the ASU is mixed with air to achieve an O_2 diluted regeneration stream, thus avoiding undesired reactions taking place in the regenerator. The syngas effluent undergoes a partial high temperature shift (HTS) and is cooled down to generate hot water for the MeOH reactor and LP steam for the purification column. The syngas at ambient temperature is then routed to a Selexol unit with a simplified scope (as H_2S has been removed upstream), where the CO_2 product is compressed and pumped to delivery pressure, while the syngas product is routed to the synthesis loop. The purge stream from the loop is fed to a pressure swing adsorption (PSA) unit to retrieve H_2, while the off-gas is combusted in a boiler for power generation in a steam cycle. Integration of the PSA enables further reduction of heat input relative to the reference plant, preventing valuable H_2 from being converted at low efficiency to electrical power by recycling it to the to the synthesis feed point, consequently maximizing fuel efficiency. Nevertheless, this process topology assumes that certain power imports to the plant are possible and therefore this configuration is not electrically self-sufficient.

Two processes are evaluated based on this line-up. In the first case (Adv. I), O_2 from the ASU is delivered at 95 %mol. purity while the purge gas from the synthesis loop is combusted in a conventional boiler, producing some CO_2 emissions. In the second case (Adv. II), the O_2 purity is increased to 98 %mol whilst producing steam in an oxy- boiler, carrying out the combustion with pure O_2 from the ASU. Increased purity of the oxidant stream from the ASU is necessary to obtain a final CO_2 stream composition within specifications for transport and storage [39], which leads to a larger power consumption of both the ASU and CO_2 compression (due to increased capture rate).

2.3. Electrolysis MeOH plants

The MeOH configurations featuring water electrolysers to produce H_2 consist of a gasification island (E-gas gasifier) operating at analogous conditions as the previous concepts. In the present schemes, since deficient H_2 can be synergistically supplied from a different source other than the solid fuel, the WGS unit (and CO_2 removal) are avoided, thereby maximizing carbon efficiency. Two process concepts with different rate of electrolytic H_2 production are considered. In the first configuration (El. I), it is assumed that after H_2S removal from syngas in the HGCU unit, compressed H_2 from the PEM unit is added to achieve suitable conditions for synthesis. Additionally, O_2 from the anode outlet is used as oxidizing agent of the gasifier after compression. Purification steps (i.e., de-oxygenator and de-hydrogenator) are integrated after the PEM, assuming 100 % pure H_2 and O_2 product outlets of the unit. The synthesis loop purge is utilized as fuel in a conventional boiler to generate steam for the power cycle, leading to some carbonaceous emissions. As mentioned, this process configuration does not require any CO_2 removal, compression, transport & storage infrastructure, since the carbon from the solid fuel blend is entirely transformed either to MeOH or CO_2 emissions. However, syngas from the gasifier still contains a substantial amount of CO_2 (~14 %mol), which results in a large H_2 demand for this arrangement to reach a syngas stoichiometry according to Eq. (1).

An alternative plant design (El. II) to reduce the size and consequently electricity consumption of the electrolyser consists of partially removing CO_2 produced by the gasification process. Since no WGS unit is implemented, a chemical absorption process with MDEA removes approximately 85 % of the CO_2, leading to a very high CO/CO_2 ratio in the feed syngas to the loop. A chemical solvent is preferred in this case due to the relatively lower CO_2 partial pressure in the syngas stream. Complete CO_2 removal is not advisable from the perspective of optimal catalyst performance [6]. The fuel purge stream from the synthesis loop is conveniently combusted in an oxy-boiler to prevent carbonaceous emissions, since a CO_2 compression unit as well as transport and storage infrastructure are present in this configuration. Furthermore, O_2

produced by the electrolyser is not sufficient to satisfy the gasifier and oxy-boiler oxidant demand, therefore a small ASU unit must be implemented.

2.4. Electrolyser model

Several electrolyzer technologies are available for H_2 production from carbon free power sources. A review of literature studies for different PtX designs is provided in Smolinka et al. [40]. Based on their operating temperature, there are two main groups of cells for water electrolysis: the high-temperature (700–850 °C) solid oxide electrolysis cells (SOEC) that split the water molecule in gaseous state, and the low-temperature cells (below 100 °C, or somewhat above under pressurized conditions) that are fed with liquid water. Among the latter, the main technologies are alkaline cells, proton exchange membrane (PEM) cells, and more recently, anion exchange membrane (AEM) cells. The high temperature cells operate with significantly lower voltage due to the enhanced electrochemical kinetics in the electrodes, leading to a low electricity consumption. However, the high operating temperatures and stresses during shutdown/ramping transitions imply a relatively fast degradation and low lifetime.
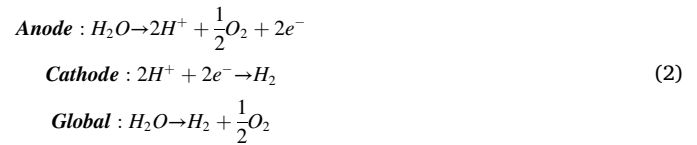
A comparison between Solid Oxide (SOEC) water electrolysis and PEM technology for MeOH production carried out by Rivera-Tonoco et al. [27] reveals that the latter is significantly more cost competitive as a result of a lower specific cost and longer component lifetime, while also facilitating more effective coupling to intermittent energy sources. Thus, low-temperature electrolysis is selected for the present study.

Alkaline electrolyzers use concentrated KOH as electrolyte and nickel (Ni) coated stainless-steel for the electrodes. A fraction of the product gases can dissolve in the electrolyte, limiting their ability to operate at higher pressure levels. Diaphragms can avoid this challenge at the cost of extra ohmic resistance and loss of efficiency. Alkaline designs are easy to manufacture, reliable and reach long lifetimes. In comparison, PEM electrolysers are based on the use of perfluorosulfonic acid (PFSA) thin membranes that facilitate a high ionic conductivity. In combination with advanced architecture of electrodes, these membranes lead to a high voltage efficiency compared with the other low-temperature technologies. As a result, PEM electrolysers can potentially operate at higher current densities for similar voltage in comparison with alkaline electrolysers, thus reducing the required electrode surface area for a given hydrogen rate of production. The PFSA membrane is also quite mechanically and chemically robust, facilitating operation with high pressure differentials between the electrodes, which can be interesting for producing hydrogen at high pressures to save compression power. PEMs have one of the most compact and simplest system designs. As drawback, typical materials used for electrodes are iridium oxide in the anode (oxygen side) and platinum nanoparticles in carbon black at cathode. The use of these expensive noble materials is required due to the highly acid environment created by the PFSA membrane. The AEM technology aims to maintain simplicity and efficiency of the PEM in combination with the use of non-noble metals for the electrodes. However, this technology is not currently mature as mechanical and chemical stability problems have been reported [41]. For the reasons discussed, the PEM technology has been chosen as the most suitable for the process under study in this work, although the use of alkaline technology would return similar techno-economic results.

A PEM electrolyser model has been developed based in data and assumptions taken from available literature. In the following subsections we provide a summary of the model. More details can be found in the supplementary material file. A good review on PEM electrolyser modelling can be found in Falcao et al. [17].

2.4.1. Electrolysers cell reversible voltage

The electrochemical reactions taking place are:

$$\textbf{Anode} : H_2O \rightarrow 2H^+ + \frac{1}{2}O_2 + 2e^-$$

$$\textbf{Cathode} : 2H^+ + 2e^- \rightarrow H_2 \tag{2}$$

$$\textbf{Global} : H_2O \rightarrow H_2 + \frac{1}{2}O_2$$

The reversible voltage of the PEM electrolyser cell, also known as open circuit voltage, is determined from the Nernst equation:

$$V_{rev} = \frac{\Delta H^\circ - T\Delta S^\circ + RTln\left(P_{H_2}P_{O_2}^{1/2}\right)}{2F} \tag{3}$$

where $\Delta H^\circ = 286.03$ kJ/mol and $\Delta S^\circ = 164.01$ J/(mol·K). Since both electrodes will be operating under wet conditions, the partial pressure of hydrogen, P_{H_2}, and oxygen, P_{O_2}, must be corrected taking into account the water content of the vapour phase, directly related with the working temperature:

$$\begin{aligned} P_{H_2} = P_{cathode} - P^v(T) \\ P_{O_2} = P_{anode} - P^v(T) \end{aligned} \tag{4}$$

2.4.2. Voltage losses

The PEM cell voltage is predicted adding the overpotentials terms due to voltage losses (electrodes activation, ohmic and concentration) to the open circuit voltage:

$$V_{cell} = V_{cell} + V_{act,anode} + V_{act,cathode} + V_{ohm} + V_{con} \tag{5}$$

2.4.3. Activation overpotential

The Butler-Volmer equation describes the relation between current and voltage in electrochemical systems and can be used to relate the current density to the voltage. It is considered the cornerstone of electrochemical kinetics [42]:

$$j = j_0\left(exp\left(\frac{\alpha n_e F V_{act}}{RT}\right) + exp\left(-\frac{(1-\alpha)n_e F V_{act}}{RT}\right)\right) \tag{6}$$

The exchange current density (j_0) is strongly dependent on temperature via an Arrhenius [17,42]:

$$j_0 = j_{0,ref}\exp\left(-\frac{E_{act}}{R}\left(\frac{1}{T} - \frac{1}{T_{ref}}\right)\right) \tag{7}$$

The values of the activation energy (E_{act}) for anode and cathode are taken from literature [43,44] (see Table 1). Although some authors have reported a certain dependence of the charge transfer coefficient with temperature [45], the usual practice is to consider it constant with temperature [17].

A wide range of values have been reported in literature for the charge transfer coefficient $(0.2 < \alpha < 2)$ and the exchange current density $(10^{-9} < j_{0,anode} < 10^{-2}; 10^{-6} < j_{0,cathode} < 10)$ in PEM electrolysers [17]. In practice, most authors rely on experimental data to adjust their models and adopt the values that best fit, and a recent experimental study [46] was used for this purpose in the present work. The values of the exchange current density and charge transfer coefficient that leads to the best adjust are given in Table 1.

2.4.4. Ohmic overpotential

Ohmic losses are described by Ohm's Law. In principle two terms may be considered, the ionic resistance of the membrane and the electronic resistance of the catalytic layer, but the latter is commonly neglected [43,47]:

$$V_{ohm} = (ASR_{ion} + ASR_{elec})j \approx ASR_{ion} \cdot j \tag{8}$$

The ionic resistance to the proton flux across the PEM is directly proportional to the membrane thickness and inversely proportional to its electric conductivity:

Table 1
Parameters of the PEM electrolyser model based in collected data for Nafion® membranes.

Symbol	Parameter	Value	Reference
$j_{0,anode}$(80 °C)	Anode exchange current density	$5.0 \cdot 10^{-8}$ A/cm^2	adjusted from [46]
α_{anode}	Anode charge transfer coefficient	0.8	adjusted from [46]
$E_{act,anode}$	Anode activation energy	76 kJ/mol	[43,44]
$j_{0,cathode}$(80 °C)	Cathode exchange current density	0.4 A/cm^2	adjusted from [46]
$\alpha_{cathode}$	Cathode charge transfer coefficient	0.25	adjusted from [46]
$E_{act,cathode}$	Cathode activation energy	18 kJ/mol	[43,44]
λ	Hydration ratio	20	[50]
δ	PEM relative thickness change	$0.1 + 0.00052(T(°C) - 23)$	[50]
k_1	EO drag coeff. correlation constant	2.15	[54,57] average
k_2	EO drag coeff. correlation constant	0.0173	[54,57] average
K_{P,H_2}(60 °C)	H$_2$ permeability coefficient	56.7 (mA/cm^2)·(µm/bar)	[27]
E_{act,P,H_2}	H$_2$ permeability activation energy	17.7 kJ/mol	[27]
f_P	H$_2$ perm. pressure enhancing factor	19 bar/(A/cm^2)	[27]
$\dot{n}_{P,O_2}/\dot{n}_{P,H_2}$	O$_2$/H$_2$ molar permeability ratio	0.5	[27,56]

$$ASR_{ion} = \frac{L}{\sigma} = \frac{L_0(1 + \delta)}{\sigma} \tag{9}$$

The membrane's ionic conductivity and the actual membrane thickness for a cell in operation is evaluated considering a thickness change from dry to water soaked. The relative thickness change (δ) increases from 10 % at 23 °C to 14 % at 100 °C, according to the Nafion® N115, N117 and N1110 product bulletin [48]. The conductivity depends on the temperature and the degree of hydration of the membrane. For Nafion® PEMs the following dependence for the ionic conductivity is well known [17,43,49]:

$$\sigma = (0.005139\lambda - 0.003260)exp\left(1268\left(\frac{1}{303} - \frac{1}{T}\right)\right) \tag{10}$$

Due to the electro-osmotic drag of water from anode to cathode both electrodes are expected to operate liquid water soaked, so the approach of taking $\lambda = 20$ has been adopted in this work, as indicated by Morawietz et al. [50] from intensive investigation with Nafion® immersed in liquid water.

2.4.5. Concentration overpotential

Concentration losses can be ignored for current densities below 1.6 A/cm^2 [17] or even 3 A/cm^2 [51]. Since these values are beyond the value used in the present study (1 A/cm^2), these losses are ignored.

2.4.6. Electro-osmotic water drag

The drag coefficient (n_d) is defined as the number of water molecules transferred per proton due to the electro-osmosis phenomenon [52]. According to Ito et al. [53], when the membrane electrode assembly is fabricated using chemical plating, for a fully hydrated membrane n_d depends only on the PEM temperature, which can be described using a linear correlation [53,54]:

$$n_d = k_1 + k_2 T (\,°C) \tag{11}$$

It has been found that ($k_1 = 3.69$, $k_2 = 0.0134$) [1] tends to

overestimate n_d, while ($k_1 = 0.6$, $k_2 = 0.0212$) [54] tends to underestimate it, but interestingly, taking the averaged value between these values leads to predictions of n_d consistent with the data provided by literature for commercially available electrolysers. For instance, for a temperature of 80 °C this method gives $n_d = 3.534$, in agreement with literature values in the range of 3.5–4 [27,46,55].

2.4.7. Gas cross permeation

Gas permeation in PEM electrolysers is an important aspect, both for safety and efficiency reasons. On the one hand, the H$_2$ content in the O$_2$ outlet stream should not reach 4 % (lower explosion limit). In addition, the efficiency of the process reduces if some of the H$_2$ produced by electrolysis is lost due to a high permeation rate. These undesirable effects are accentuated in the case that the cathode operates at high pressure. The O$_2$ permeation rate is known to be about half that of H$_2$ in Nafion® PEMs [2,3]. For that reason, together with a certain catalytic recombination between permeated O$_2$ and H$_2$ at the cathode by the action of Pt, the cathode-to-anode hydrogen permeation rate is the key element to be monitored.

To evaluate H$_2$ permeation rate, the method presented by Papakonstantinou et al. [56] is applied. In terms of equivalent current, hydrogen losses by permeation for a Nafion® membrane are given as a function of hydrogen partial pressure in the cathode, temperature, and current density of the cell:

$$j_{P,H_2} = K_{P,H_2} exp\left(-\frac{E_{act,P,H_2}}{R}\left(\frac{1}{T} - \frac{1}{333K}\right)\right)\frac{P_{H_2,cathode} + f_P \cdot j}{L} \tag{12}$$

where $K_{P,H_2} = 56.7$ (mA/cm^2)·(µm/bar), $E_{act,P,H_2} = 17.7$ kJ/mol, and $f_P = 19$ bar/(A/cm^2). Considering that the O$_2$ permeation rate is half that of H$_2$ and that every O$_2$ permeated molecule will recombine with two H$_2$ molecule at cathode side, the net hydrogen molar flow per unit area that is finally obtained at the system outlet (less the gas cross permeation losses), is given by:

$$\left(\frac{\dot{n}_{H_2,net}}{A}\right) = \frac{j}{2F}\left(1 - \frac{1.25j_{P,H_2}}{j}\right) \tag{13}$$

2.4.8. PEM stack performance

The electrode surface area required for a given net hydrogen molar flow can be obtained from Eq. (13):

$$A = \frac{2F\dot{n}_{H_2,net}}{j\left(1 - \frac{1.25j_{P,H_2}}{j}\right)} \tag{14}$$

The power consumption of the stack is then calculated as:

$$\dot{W}_{stack} = (j \cdot A) \cdot V_{cell} = \frac{2F\dot{n}_{H_2,net}V_{cell}}{1 - \frac{1.25j_{P,H_2}}{j}} \tag{15}$$

2.4.9. Electrolyser system and balance of plant

PEM electrolysers are considered simpler and more operationally flexible than the alkaline technology counterpart [41]. A process flowsheet has been developed in UniSim Design® to represent the main components of the electrolyser system according to Fig. 4. Fresh water passes through a deionizer to purify and condition it for electrolysis. Afterwards, the main water pump pressurizes to feed the PEM stack. Downstream, the anodic O$_2$/water and the cathodic H$_2$/water streams are directed to two-phase separators, removing most of the water content of both streams. Due to the cross-gas permeation, a certain amount of H$_2$ is still present in the cathodic gas stream, and similarly impurities of O$_2$ occur in the cathodic stream. Since a high H$_2$ purity is required for chemical synthesis, a catalytic recombination is induced in a deoxidizer reactor to eliminate O$_2$ impurities. In most applications, purification of the O$_2$ stream is not mandatory, but this is not the case for the process under study in this work, as highly pure O$_2$ is desirable for gasification
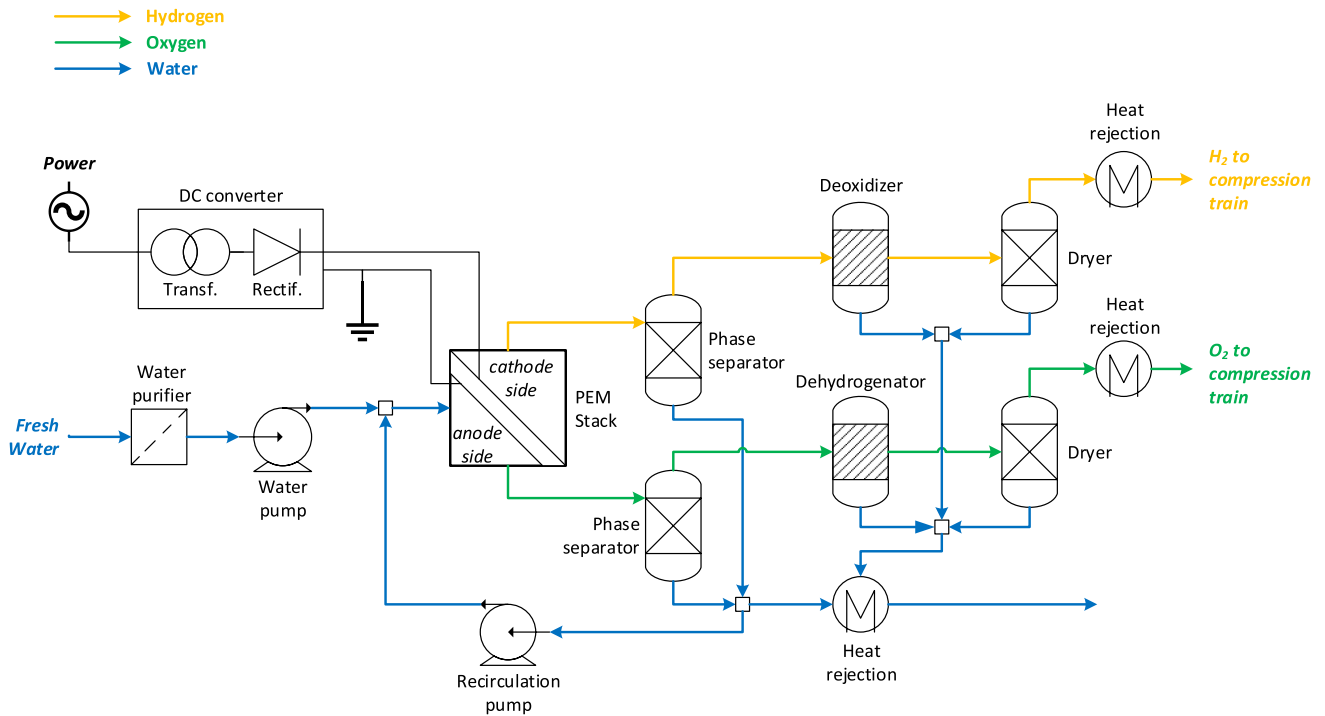
Fig. 4. PEM electrolyser system design.

and furthermore the presence of H_2 poses safety concerns during compression. For that purpose, a dehydrogenator reactor is deployed. After the catalytic purification, both streams are dehydrated achieving dry streams of pure H_2 and O_2.

The temperature in the PEM stack is controlled by the circulation of excess water to the anode inlet. The temperature difference imposed between inlet and outlet streams is $\Delta T = 10^{\circ}C$, as proposed by Rivera-Tinoco et al. [27]. After evaluation of the power consumption by the stack model (Eq. (15)), the UniSim flowsheet calculates the excess water required to remove the heat released in the stack due to energy losses, as sensible heat related to the specified ΔT. For optimal heat recuperation, the hot water obtained from the two-phase separators is recirculated to the stack to preheat the water feed inlet to the stack. This system scheme is very similar to the typical system design for a PEM electrolyser depicted in IRENA's report [41].

The PEM stack is powered by DC electric current, therefore an AC/DC converter (transformer & rectifier) is required for that purpose. This electronic DC converter is responsible for the main auxiliary consumption of the electrolyser. According to recent literature [58], the current state-of-art (year 2022) of DC converters for large-scale hydrogen production from water electrolysis is > 94 % with a forecast of reaching > 98 % in the future. Since this work intends to assess the future viability of a novel methanol synthesis processes to be deployed around year 2050, an intermediate value of $\epsilon_{AC/DC} = 96\%$ has been selected to estimate the energy consumption of the converter. The total electrolyser system power consumption is determined as follows:

$$\dot{W}_{electrolyser} = \frac{\dot{W}_{stack}}{\epsilon_{AC/DC}} + \dot{W}_{pumping} \quad (16)$$

Overall, the pumping duty is negligible compared to the stack power consumption, therefore pressure losses across the stack system were not accounted for and recirculation duty is neglected. This is an acceptable assumption, given the very small pressure drops encountered in these systems [59]. On the other hand, product compression to process unit requirements is considered separately.

2.5. Plant performance indicators

In this section, the key performance indicators for the plants are defined to provide a detailed understanding of each configuration from an energy, environmental and economic perspective.

2.5.1. Energy & environmental

Energy efficiency reflects the fuel conversion performance to MeOH product and is treated differently for the plants without and with electrolysers. For the plants employing only solid fuels as primary energy feedstock, the methanol production efficiency (η_{MeOH}) is defined according to Eq. (17). To consistently account for electricity imports or exports of the plant, an equivalent efficiency ($\eta_{MeOH,eq}$) is defined assuming a reference heat to power conversion ratio of a natural gas combined cycle (62.3 %) [60], as shown in Eq. (18), where $\dot{W}_{net}$ is positive for exports. Finally, electrical efficiency ($\eta_{El.}$) considers the ratio between the net electrical power and fuel heat input (Eq. (19)).

$$\eta_{MeOH} = \frac{\dot{m}_{MeOH}LHV_{MeOH}}{\dot{m}_{coal}LHV_{coal.} + \dot{m}_{bio}LHV_{bio}} \quad (17)$$

$$\eta_{MeOH,eq} = \frac{\dot{m}_{MeOH}LHV_{MeOH}}{\dot{m}_{coal}LHV_{coal.} + \dot{m}_{bio}LHV_{bio} - \frac{\dot{W}_{net}}{\eta_{ref}}} \quad (18)$$

$$\eta_{El.} = \frac{\dot{W}_{net}}{\dot{m}_{coal}LHV_{coal.} + \dot{m}_{bio}LHV_{bio}} \quad (19)$$

The specific consumption as defined in Eq. (20) reflects the primary energy requirements per ton of MeOH product. Similarly, an equivalent specific consumption accounts for electricity imports and exports (Eq. (21)).

$$SC = \frac{\dot{m}_{coal}LHV_{coal.} + \dot{m}_{bio}LHV_{bio}}{\dot{m}_{MeOH}} \quad (20)$$

$$SC_{eq} = \frac{\dot{m}_{coal}LHV_{coal.} + \dot{m}_{bio}LHV_{bio} - \frac{\dot{W}_{net}}{\eta_{ref}}}{\dot{m}_{MeOH}} \quad (21)$$

The carbon efficiency (ε_C) is an insightful metric defined in Eq. (22)

as the fraction of carbon from the solid fuel blend transformed to MeOH product. A high carbon efficiency is desirable since it reflects a high fuel conversion performance through minimization of losses in the form of captured and emitted CO_2.

$$\varepsilon_C = \frac{\dot{n}_{C,MeOH}}{\dot{n}_{C,coal} + \dot{n}_{C,bio}} \qquad (22)$$

In terms of environmental performance, the specific CO_2 emissions (E_{CO_2}) are defined in Eq. (23). Negative emissions are achieved if the biogenic CO_2 capture exceeds the fossil CO_2 emitted. Furthermore, a total CO_2 emission metric is defined where the MeOH product is assumed to be combusted at end use and the resulting CO_2 emissions from fossil origin are emitted to the atmosphere (Eq. (24)). Furthermore, the specific capture (C_{CO_2}) underlines the extent to which carbon atoms must be removed from the syngas per mass unit of MeOH product, as shown in Eq. (25).

$$E_{CO_2} = \frac{\dot{m}_{CO_2,emit.}^{coal} - \dot{m}_{CO_2,capt.}^{bio}}{\dot{m}_{MeOH}} \qquad (23)$$

$$E_{CO_2,tot} = \frac{\dot{m}_{CO_2,emit.}^{coal} - \dot{m}_{CO_2,capt.}^{bio} + \dot{m}_{MeOH}\frac{M_{r,CO_2}}{M_{r,MeOH}}\frac{\dot{n}_{C,coal}}{\dot{n}_{C,coal}+\dot{n}_{C,bio}}}{\dot{m}_{MeOH}} \qquad (24)$$

$$C_{CO_2} = \frac{\dot{m}_{CO_2,capt.}^{coal} + \dot{m}_{CO_2,capt.}^{bio}}{\dot{m}_{MeOH}} \qquad (25)$$

For plants delivering H_2 through an electrolyser, the definitions of energy efficiency and specific consumption are redefined in Eq. (26) - Eq. (29), accounting the power input to the electrolyser as primary energy as such plants will only be built where clean electricity is very cheap. In the calculation of equivalent metrics, the net auxiliary electricity consumption incurred upon by the remaining plant units is added directly, without the power to heat conversion factor previously taken into account.

$$\eta_{MeOH} = \frac{\dot{m}_{MeOH}LHV_{MeOH}}{\dot{m}_{coal}LHV_{coal.} + \dot{m}_{bio}LHV_{bio} - \dot{W}_{El.}} \qquad (26)$$

$$\eta_{MeOH,eq} = \frac{\dot{m}_{MeOH}LHV_{MeOH}}{\dot{m}_{coal}LHV_{coal.} + \dot{m}_{bio}LHV_{bio} - \dot{W}_{El.} - \dot{W}_{net}} \qquad (27)$$

$$SC = \frac{\dot{m}_{coal}LHV_{coal.} + \dot{m}_{bio}LHV_{bio} - \dot{W}_{El.}}{\dot{m}_{MeOH}} \qquad (28)$$

$$SC_{eq} = \frac{\dot{m}_{coal}LHV_{coal.} + \dot{m}_{bio}LHV_{bio} - \dot{W}_{El.} - \dot{W}_{net}}{\dot{m}_{MeOH}} \qquad (29)$$

2.5.2. Economic

An economic assessment of all the cases is carried out through a consistent capital and operational cost estimation, with the cost basis for the evaluation defined in Table 2. The Standardized Economic Assessment tool [61] developed by the authors is employed for such purpose, and a comprehensive user manual can be found in [62]. Detailed results for each case are available for download [63].

The bare erected cost (BEC) estimation of each plant unit relies on equipment correlations developed by Turton [64] and/or simplified cost-capacity scaling cost estimations for an extended scope of the plant, based on published literature references [28,30,65]. From the BEC estimate, the total overnight cost is determined by applying the methodology detailed in Table 3. No process contingency (PC) for conventional

Table 2

Cost basis details.

Location	Western Europe
Year	2020
Currency	€

Table 3

Economic assumptions [28,30].

Capital estimation methodology	
Bare Erected Cost (BEC)	SEA Tool Estimate
Engineering Procurement and Construction (EPC)	10 % BEC
Process contingency (PC)	0–30 % BEC
Project Contingency (PT)	20 % (BEC + EPC + PC)
Owners Costs (OC)	15 % (BEC + EPC + PT + PC)
Total Overnight Costs (TOC)	BEC + EPC + PC + PT + OC

Operating & maintenance costs		
Fixed		
Maintenance	2.5	%TOC
Insurance	1	%TOC
Labour	60,000	€/y-p
Operators	120	Persons
Variable		
Coal	2.5	€/GJ
Biomass	100	€/ton
Electricity	60	€/MWh
Oxygen carrier	15	€/kg
MeOH catalyst	30	€/kg
WGS catalyst	16,100	$/ton
CO_2 tax	100	€/ton
CO_2 transport & storage	20	€/ton
Process water	6	€/ton
Cooling water make-up	0.35	€/ton
Ash disposal	9.73	€/ton
Absorbent make-up	5000	€/ton

Cash flow analysis assumptions		
1st year capacity factor	65	%
Remaining years	85	%
Discount Rate	8	%
Construction period	4	years
Plant Lifetime	25	years

technologies already deployed at large scale is assumed. However, a 10 % contingency for technology step-outs within the scope of a unit such as slurry vaporization in the E-gas gasifier and oxy-combustion boilers in the power cycle is taken, respectively. Furthermore, given the stringent constraints in sulphur levels imposed by the chemical synthesis, pre-commercial stage of this technology and challenges related to inter-connected fluidized bed operation at high pressures, a 30 % PC was assumed for the HGCU unit. On the other hand, fixed (FOM) & variable (VOM) operating and maintenance costs are determined consistently to previous studies [14]. Finally, a set of economic premises is defined for a coherent cash flow analysis of the different MeOH production processes.

Furthermore, this study presents a dedicated cost estimation of the electrolyser and downstream purification steps. This evaluation was performed via a bottom-up assessment of PEM electrolyzer costs for the year 2050 based on an NREL assessment of a fully scaled global supply chain producing 50 GW of electrolyzers per year. More details can be found in the Supplementary Material. An optimization of membrane thickness and operating current density was carried out to achieve the lowest H_2 production cost. For illustration, the electrolyser unit from El. I plant reaches a specific total overnight cost of 586.8 €/kW of H_2 (of which approximately 77.1 % corresponds to the stack) and an efficiency of 70.92 % (LHV), for production at 10 bar and 110 °C. This high operating temperature is possible as the anode side works also under the same pressurized conditions, ensuring a circulation of liquid water across the cells to maintain the PEM conveniently hydrated. In the economic assessment of the cases including electrolysis, a membrane replacement is assumed at the plant year 13, according to the lifetime projections for this technology.

The levelized cost of product (*LCOP*) is defined as the selling price at which the net present value (Eq. (30)) of the plant becomes zero, while the latter is the summation of the discounted annual cash flows (Eq.

(31)) across the plant lifetime; calculated accounting for revenues of product (P_{MeOH}) and variable (C_{VOM}) costs which are dependent on plant capacity factor (ϕ), in addition to fixed (C_{FOM}) and capital costs ($C_{Capital}$).

$$NPV = \sum_{t=0}^{n} \frac{ACF_t}{(1+i)^t} \qquad (30)$$

$$ACF_t = \phi \cdot (LCOP \cdot P_{MeOH} - C_{VOM}) - C_{Capital} - C_{FOM} \qquad (31)$$

Several sensitivity analyses are carried out to underline the robustness of the economic assessment with respect to key assumptions. Namely, the fuel price of biomass and coal feedstocks, the transport and storage costs of CO_2 and respective emissions taxes, which result in an additional plant revenue for cases with CCS achieving negative emissions, as well as electricity and gasifier costs variations are considered to provide a holistic overview of the economic performance of each configuration.

3. Results

Results are presented in two sections. First, plant energy and environmental performance results for all cases is given. Then, the economic results are shown, alongside suitable sensitivity analysis to key economic assumptions.

3.1. Energy & environmental results

The energy and emissions performance for the five plants is provided in Table 4 based on the metrics defined in the preceding section. Relative to the reference plant, Adv. I and II see strong improvements in efficiency, mainly related to the high CGE of the E-gas relative to the GE gasifier. In addition to reducing fuel demand, more efficient gasification also reduces the power demand of the ASU (due to lower O_2 demand) and CO_2 capture and compression (due to less CO_2 formed during combustion with O_2), but it reduces heat production and subsequent steam turbine output.

The high CO_2 production of Ref. gives it greater negative emissions than Adv. I. However, through integration of an oxy-boiler and higher purity O_2 generation for achieving near 100 % CO_2 capture, Adv. II attains even more negative emissions than Ref. Capturing all the produced CO_2 not only increases the amount of biogenic CO_2 stored, but also reduces the amount of fossil CO_2 emitted, achieving a large benefit for a relatively small increase of the specific capture ratio relative to Adv. I.

As outlined in Eq. (26) - Eq. (29), the plants integrating electrolyser technology (El. I and II) present an additional primary energy feedstock in terms of electricity for water electrolysis, which is treated equivalently to the solid fuel input. Methanol production efficiencies are at a similar level to the Adv. I and II plants, indicating that the losses in converting electricity to hydrogen are similar to those involved in converting solid fuels to syngas. However, the losses in electrolysis are slightly higher as indicated by the 2.5 %-points lower efficiency of El. I relative to El. II, which has a 35.5 % lower electrolyzer duty. In addition, El. II achieves negative emissions due to the added CCS scope (absorption unit and oxy-boiler), whereas El. I has positive emissions resulting from the combustor. However, as Fig. 2 clearly shows, El. I brings significant practical benefits in terms of plant simplicity and avoidance of the need to handle CO_2.

3.2. Economic results

The economic results for the different MeOH production processes are presented in the subsequent sub-sections. A comprehensive comparison with conventional transportation fuels is provided to underline the potential of MeOH in this sector.

3.2.1. Economic assessment and cash flow analysis

The specific total overnight cost, estimated as detailed in Table 3, is presented in Fig. 5. The improved gasification efficiency of the Adv. I and II plants allow for smaller gasifiers and ASUs relative to the reference plant. When electrolysis is added in El. I and II, the combined gasifier and electrolyzer costs reach a similar level to the gasifier and
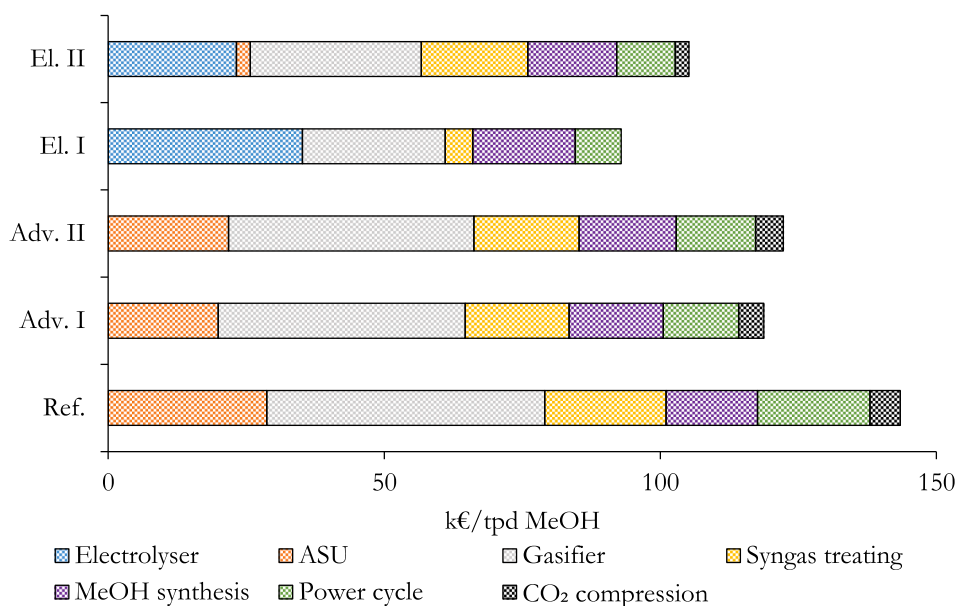
Table 4
Energy and environmental results for the MeOH plants.

Item	Units	Ref.	Adv. I	Adv. II	El. I	El. II
Heat flow breakdown						
H_2 heat input	MW$_{th}$	0.0	0.0	0.0	1364.2	880.1
H_2 flow rate	kg/s	0.0	0.0	0.0	11.4	7.3
Blend heat input	MW$_{th}$	4300.5	3594.6	3500.1	1744.5	2291.2
Blend flow rate	kg/s	190.7	159.4	155.2	77.4	101.6
MeOH LHV	MW$_{th}$	2273.2	2290.3	2278.1	2276.3	2279.5
MeOH prod.	tpd	9988.5	10064.3	10008.4	10002.6	10017.7
Power breakdown						
ASU	MW$_{el}$	210.2	131.2	146.2	0.0	13.9
Syngas treating	MW$_{el}$	66.3	35.7	34.6	1.1	5.1
Pumps	MW$_{el}$	8.5	3.8	3.7	1.8	2.3
Blower	MW$_{el}$	3.2	2.9	2.3	1.3	1.3
Syngas comp.	MW$_{el}$	15.9	15.9	16.8	24.0	14.9
Heat rejection	MW$_{el}$	6.4	4.1	4.3	3.1	3.3
Gasifier aux.	MW$_{el}$	11.5	9.6	9.4	15.1	19.8
CO_2 comp.	MW$_{el}$	59.4	40.3	48.8	0.0	25.0
H_2 comp.	MW$_{el}$	0.0	0.0	0.0	40.2	25.9
Total aux.	MW$_{el}$	−381.4	−243.4	−266.1	−86.5	−111.3
Steam turbine	MW$_{el}$	444.6	211.9	198.5	106.9	139.2
Electrolyser duty	MW$_{el}$	0.0	0.0	0.0	−1923.5	−1240.9
Net plant	MW$_{el}$	63.2	−31.5	−67.6	−1903.2	−1213.1
Key performance indicators						
η_{MeOH}	%	52.9	63.7	65.1	62.1	64.5
$\eta_{MeOH,eq}$	%	54.1	62.8	63.1	62.4	65.0
$\eta_{El.}$	%	1.5	−0.9	−1.9	–	–
E_{CO_2}	kg/ton	−320.0	−151.1	−358.7	100.8	−130.8
$E_{CO_2,tot}$	kg/ton	744.5	913.1	705.9	1165.3	933.7
C_{CO_2}	kg/ton	2102.9	1447.0	1607.0	0.0	591.6
ε_c	%	36.8	45.2	46.2	90.8	69.2
SC	GJ/ton	37.2	30.9	30.2	31.7	30.5
SC_{eq}	GJ/ton	36.3	31.3	31.2	31.5	30.2

Fig. 5. Specific total overnight cost for the MeOH plants.

ASU costs of the Adv. I and II plants. However, the El. I plant achieves a considerable saving in the syngas treating section as no CO_2 capture is required (which also avoids CO_2 compressors). Power cycle costs scale with the amount of high-grade heat available for raising steam. All the losses related to electrolysis occur at low temperatures unsuitable for steam generation, resulting in low power cycle costs but also low steam turbine output (Table 4). Ref. has the largest power cycle due to the large amount of steam generated in the radiant syngas cooler of the GE gasifier.

Regarding operating costs, Fig. 6 shows that primary energy inputs represent the major cost components. Clearly, the unit cost of electricity is far higher than that of coal and biomass according to the base assumptions in Table 3. FOM costs scale with the capital costs shown in Fig. 5, while VOM consists largely of CO_2 transport and storage costs and is therefore linked to the specific capture.

(C_{CO_2}) in Table 4. Revenues (negative costs) from the CO_2 tax is achieved by the plants with negative emissions, while the positive emissions of El. I results in a positive CO_2 cost.

The levelized cost of MeOH (LCOM) for the five configurations is

provided in Fig. 7. Operating costs (Fig. 6) play a larger role than capital costs (Fig. 5). Hence, the capital cost savings achieved by the addition of electrolysis cannot make up for the large increase in energy input costs in the form of costly electricity. Relative to the reference plant, Adv. I and II attain a 30.5 and 40.5 €/ton (10.7 and 14.2 %) overall levelized cost reduction, respectively. Despite larger capital cost and increased electricity imports, Adv. II outcompetes Adv. I by 10.0 €/ton (3.9 %) due to a lower fuel intake and enhanced negative CO_2 emissions. On the other hand, El. I and II present an LCOM increase of 163.3 and 77.5 €/ton (57.2 and 27.1 %) relative to the reference plant, resulting from the large electricity imports necessary to power the electrolysers.

For perspective, other studies of advanced MeOH production pathways from solid fuels report comparable LCOM values in the range of 216–260 €/ton ([10,11,12]). A study on a biomass-electrolysis hybrid plant [23] reveals an LCOM of 590.3 €/ton at an average electricity price of 38.5 €/MWh and an 80 % electrolyser capacity factor. The small scale of the plant (only 5 % that of the present study) contributed to the relatively high LCOM. On the other hand, Chen et al. [66] reveal high LCOM numbers of 712.7 and 1126.7 €/ton for coal and biomass fuelled
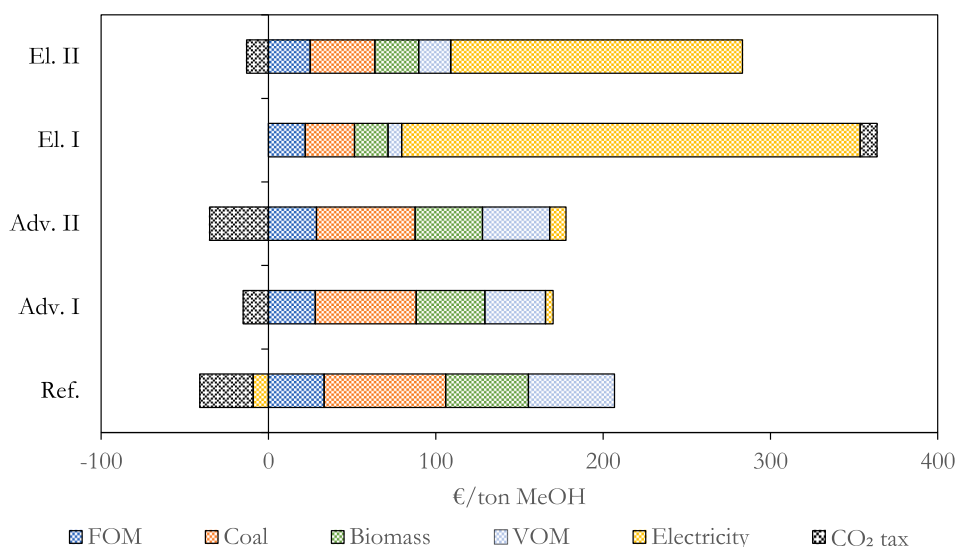

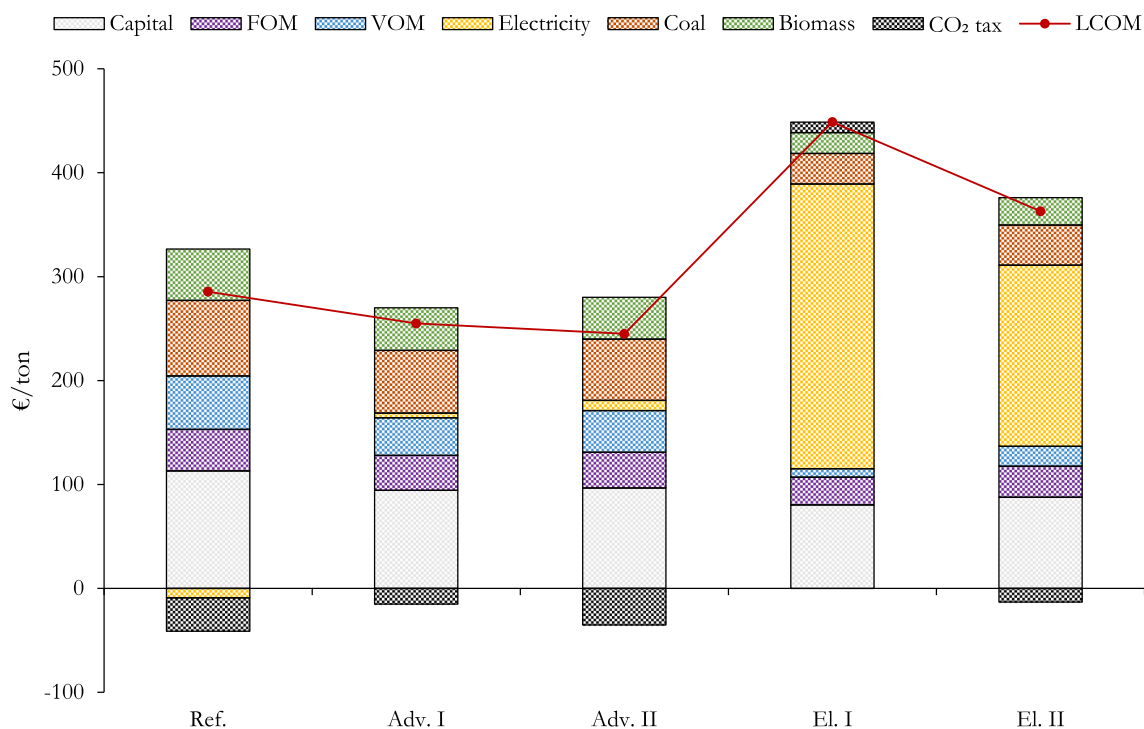**Fig. 6.** Specific operational cost for the MeOH plants.

Fig. 7. LCOM for the MeOH plants.

plants with solar powered electrolysis when using present-day solar PV technology. However, competitiveness could be achieved with elevated CO_2 taxes and future solar PV cost reductions below 30 €/MWh [66], which is in line results from the present study.

3.2.2. Sensitivity analysis

Sensitivity analyses to key economic assumptions are shown in Fig. 8. Naturally, coal and biomass prices have a greater influence on plants without electrolysis, with the reference plant being the most sensitive due to its relatively low efficiency. Still, the high cost of electricity keeps the LCOM of El. I and II well above that of the other plants even at the highest coal and biomass prices.

The sensitivity study for CO_2 emissions tax is proportional to the specific emissions of each plant shown in Table 4, with the plants achieving negative emissions benefitting from higher CO_2 taxes. Adv. I and II break even at a CO_2 price of approximately 50 €/ton, where the additional CO_2 revenues attained by the latter offset its increased capital and electricity costs. In terms of CO_2 transport and storage cost variations, El. I is unaffected as no CCS technology is implemented, while El. II is only mildly sensitive due to its low CO_2 capture rate. The reference plant is the most sensitive due to its high CO_2 production, while Adv. II is the next most sensitive due to its high capture ratio. Notably, Adv. II remains more competitive than Adv. I across the investigated range.

Naturally, the plants involving electrolysis are critically affected by the electricity price, whereas the other plants are comparatively minimally affected. El. I and El. II require an electricity price as low as 25.6 and 34.7 €/MWh respectively to break even with the reference plant. While such electricity prices may be possible for an intermittent supply of wind and solar power in certain world regions, it is unlikely that such low prices can be reached for the steady electricity supply required in this case.

Finally, a sensitivity analysis to the gasifier cost is presented, given the economic estimation uncertainty that these complex plant components presents across different literature sources [28,30,65]. Even though this uncertainty has a significant effect on the LCOM of all plants, especially those without electrolysis, it does not affect the ranking.

3.2.3. Benchmarking against alternative production pathways and gasoline

The results in Fig. 7 can be directly compared to results for methanol produced from renewables and natural gas assessed in a prior study completed using an identical methodology [7]. For additional perspective, costs and emissions related to gasoline are also shown. Gasoline costs were derived from historical data of American wholesale gasoline[1] and oil[2] prices, finding that the average gasoline price from oil at 60 €/barrel (11.1 €/GJ) is 14.7 €/GJ. Direct gasoline CO_2 emissions amount to 73 kg/GJ[3] with refining adding another 7 kg/GJ [67].

The resulting comparison is shown in Fig. 9. The Adv. II plant compares favourably with competitors, partly due to its low emissions. When coal and biomass are used as fuel, total emissions are reduced both via negative emissions from capturing and storing CO_2 and because only part of the carbon in the produced methanol is from fossil origin. For this reason, the total CO_2 emissions from the Adv. II plant is less than half that of natural gas-fuelled GSR alternative. Even though GSR achieves lower direct costs, these emissions benefits make the Adv. II plant the cheapest option for producing methanol in Europe. Furthermore, the Adv. II plant provides valuable energy security benefits by using locally produced solid fuels instead of imported natural gas.

It is also interesting to compare the El. I configuration to the pure green MeOH production system simulated previously [7]. Even though the optimally deployed and high-quality Spanish wind and solar resources returned a levelized cost of electricity of only 34 €/MWh in the green case (using mid-century technology costs), large additional costs came from the oversizing of electrolyzers for operating at a low-capacity factor with wind and solar, the direct air CO_2 capture facility, and optimized storage capacity for hydrogen, CO_2 and heat. Due to all these added costs, the El. I configuration using a steady stream of electricity at
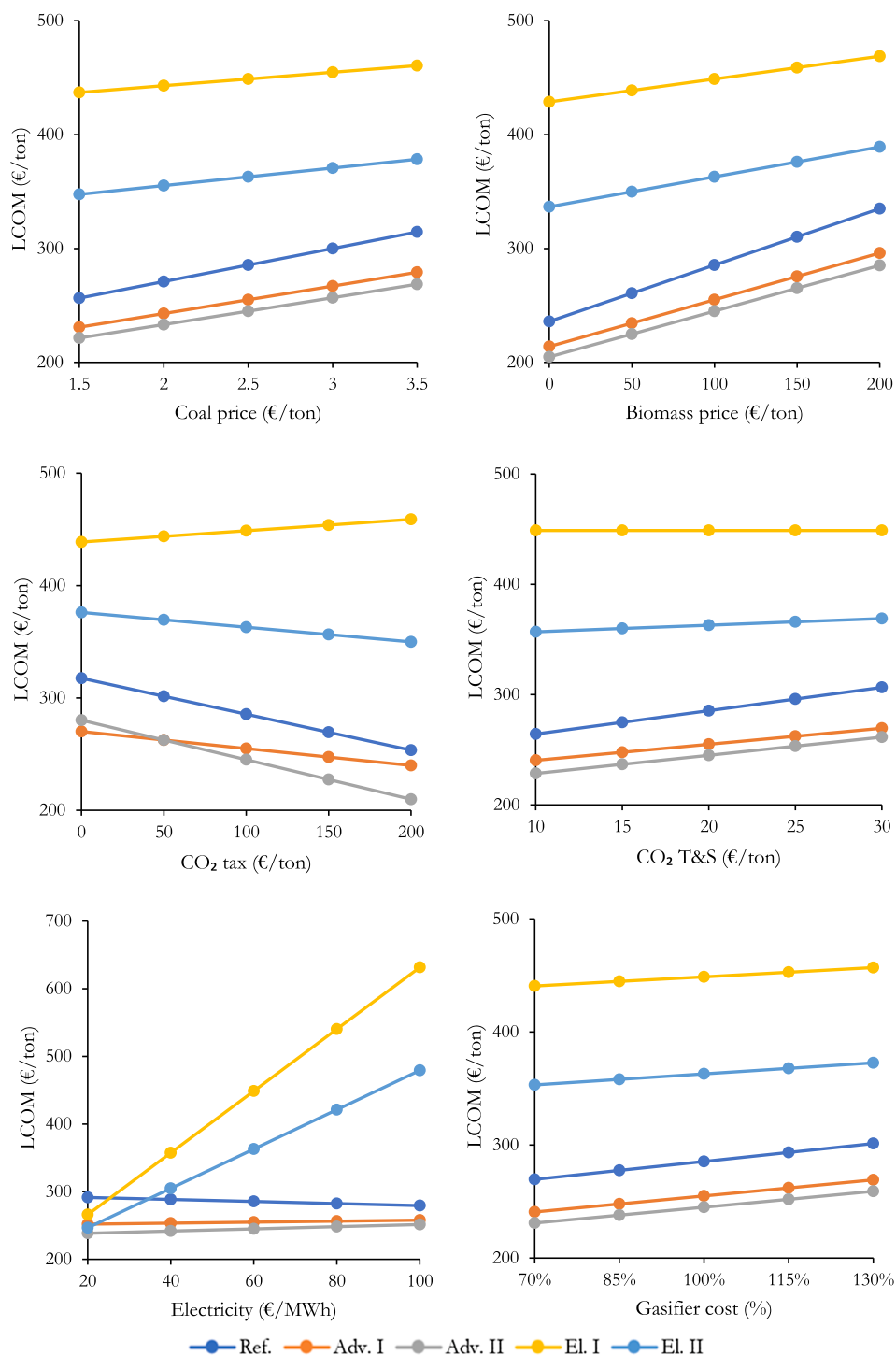

Fig. 8. Sensitivity analysis to key economic assumptions for the MeOH plants.

60 €/MWh returned considerably lower costs than the pure green alternative. In addition to avoiding multiple costs related to an intermittent electricity supply, the El. I case also benefits from using fixed carbon from solid fuels instead of CO_2 captured from the air.

When comparing to the import options, locally produced MeOH from Adv. II can be cheaper than imported gasoline from oil at 60 €/barrel. Thus, the energy security offered by locally produced MeOH would come at no cost. The main drawback of MeOH relative to gasoline as a transport fuel is that its volumetric energy density is only about half as high. However, with increasingly efficient engines, the increased fuel tank size should be manageable. MeOH produced using cheap Middle

Eastern natural gas can be cheaper than locally produced MeOH from solid fuels. However, MeOH as an easily storable liquid fuel will trade on a global market like oil where the price is set by the costliest producer. Hence, European buyers will not have direct access to the low production costs of natural gas exporting regions.

4. Summary & conclusions

In this work, five MeOH plants from solid fuels were developed and assessed from a techno-economic perspective: a reference plant (Ref.), two advanced concepts (Adv. I and II) employing more efficient gasifi-
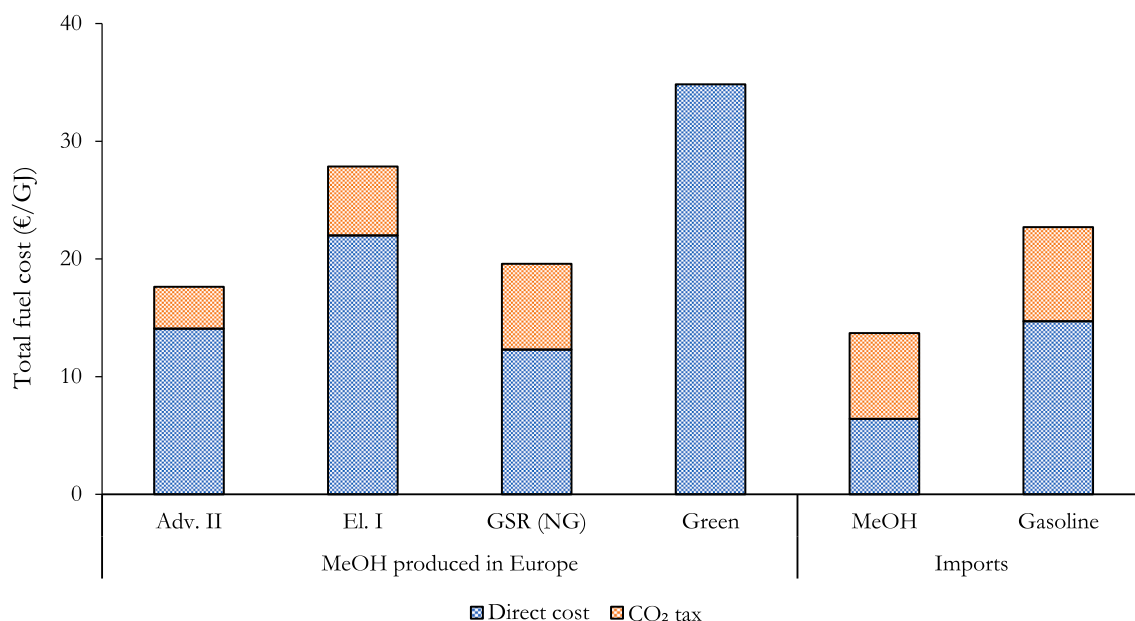
Fig. 9. A European mid-century comparison of costs and emissions for methanol production from solid fuels (represented by Adv. II), solid fuels combined with electrolysis (represented by El. I), natural gas at 6.5 €/GJ via the gas switching reforming technology, and renewable energy from high quality wind and solar resources in Spain and CO_2 captured from the air. In addition, imported methanol from Middle Eastern natural gas at 2 €/GJ and gasoline from oil at 60 €/barrel are also shown. CO_2 emissions include combustion in a transport application (i.e., $E_{CO_2,tot}$ in Table 4) and is taxed at 100 €/ton.

cation and treating technologies, and two schemes integrating an electrolyser (El. I and II) to supply H_2 to the syngas and O_2 to the gasification, thereby reducing the plant scope and solid fuel heat input relative to the first three configurations. The main outcomes of the study are summarized below:

- In terms of energy performance, Ref. attained an equivalent specific consumption (SC_{eq}) of 36.3 GJ/ton and a carbon efficiency (ε_C) of 36.8 %. Adv. I and II decreased SC_{eq} by 13.8–14.2 %, while increasing ε_C by 8.5–9.4 %-points, mainly due to more efficient gasification. El. I and II achieved similar reductions in SC_{eq} of 13.2–16.8 %, but ε_C was much higher at 69.2–90.8 % as the addition of electrolytic H_2 allowed more of the fixed carbon in the solid fuels to be utilized for MeOH production.
- Co-gasification of coal with 30 %w. biomass achieved negative emissions in plants integrating CCS. Specifically, Adv. II with an oxyboiler to capture CO_2 from combustion of the MeOH loop purge attained specific emissions (E_{CO_2}) as low as −358.7 kg_{CO2}/ton_{MeOH} compared to −320.0 kg/ton for the reference plant. El. I, which adds enough H_2 to the syngas to avoid the need CCS, showed positive emissions of 100.8 kg/ton from the MeOH purge combustor.
- From an economic standpoint, Ref. reached a levelized cost of MeOH (LCOM) of 285.5 €/ton, while Adv. I and II concepts reached 245–255.0 €/ton. Due to large electricity imports at 60 €/MWh, El. I and II showed much higher costs of 363.0–448.8 €/ton. Electricity prices as low as 25.6–34.7 €/MWh are required for these plants to break even with Ref.
- An analysis of the economic-environmental performance of MeOH as a transportation fuel showed that Adv. II could produce fuel at a similar cost to gasoline produced from oil at 60 €/barrel. However, total emissions (including fuel combustion) from MeOH produced via Adv. II are only 44 % that of gasoline, creating a clear advantage when CO_2 taxes are applied.

In conclusion, this study underlines the economic and environmental potential of both thermal efficiency improvements and blending of coal with carbon neutral fuels such as biomass in MeOH processes, when CO_2 emissions taxes are accounted for in the evaluation. Despite the

synergies with gasification and lower plant capital costs, hybridization of solid-fuel MeOH production using electrolysis requires an unrealistically low-cost supply of steady-state clean electricity to be competitive, especially if CCS is to be avoided.

The cost-competitiveness and emissions reductions of MeOH from coal-biomass co-gasification relative to gasoline offers an attractive solution to both climate change and energy security in energy importing regions like Europe. Advanced co-gasification plants such as those proposed in this work may be the most efficient way to utilize limited supplies of sustainably produced biomass for the benefit of the local economy, in terms of affordability and security, and the global economy, regarding climate change mitigation and liquid fuel market stability.

CRediT authorship contribution statement

Carlos Arnaiz del Pozo: Conceptualization, Methodology, Formal analysis, Investigation, Writing – original draft. **Ángel Jiménez Álvaro:** Conceptualization, Formal analysis, Investigation, Writing – original draft, Funding acquisition. **Schalk Cloete:** Conceptualization, Methodology, Formal analysis, Investigation, Writing – original draft, Writing – review & editing.

Declaration of Competing Interest

The authors declare that they have no known competing financial interests or personal relationships that could have appeared to influence the work reported in this paper.

Data availability

The article contains a link to the full techno-economic assessment files.

Acknowledgements

This research received funding from the European Union NextGenerationEU, Ministerio de Universidades grant RD 289/2021.

Appendix A. Supplementary data

Supplementary data to this article can be found online at https://doi.org/10.1016/j.enconman.2022.116272.

References

[1] Masson-Delmotte V, Zhai P, Pörtner H, Roberts D, Skea J, Shukla PR, et al. "Global Warming of 1.5 OC: An IPCC Special Report on the Impacts of Global Warming of 1.5° C Above Pre-industrial Levels and Related Global Greenhouse Gas Emission Pathways, in the Context of Strengthening the Global Response to the Threat of Climate Change. Sustainable Development, and Efforts to Eradicate Poverty" 2018.

[2] IEA, "World Energy Outlook. 2021, International Energy Agency." 2021.

[3] Collodi G, Azzaro G, Ferrari N, Santos S. Demonstrating large scale industrial CCS through CCU–a case study for methanol production. Energy Procedia 2017;114: 122–38.

[4] Verhelst S, Turner JW, Sileghem L, Vancoillie J. Methanol as a fuel for internal combustion engines. Prog Energy Combust Sci 2019;70:43–88.

[6] Bozzano G, Manenti F. Efficient methanol synthesis: Perspectives, technologies and optimization strategies. Prog Energy Combust Sci 2016;56:71–105.

[7] Arnaiz del Pozo C, Cloete S, Jiménez Álvaro Á. Techno-economic assessment of long-term methanol production from natural gas and renewables. Energy Convers Manage 2022;266:115785.

[8] Khalafalla SS, Zahid U, Abdul Jameel AG, Ahmed U, Alenazey FS, Lee C. Conceptual Design Development of Coal-to-Methanol Process with Carbon Capture and Utilization. Energies 2020;13:no. 23.

[9] Mondal P, Dang GS, Garg MO. Syngas production through gasification and cleanup for downstream applications — Recent developments. Fuel Process Technol 2011; 92(8):1395–410.

[10] Zhang D, Duan R, Li H, Yang Q, Zhou H. Optimal design, thermodynamic, cost and CO2 emission analyses of coal-to-methanol process integrated with chemical looping air separation and hydrogen technology. Energy 2020;203:117876.

[11] Xiang D, Li P, Yuan X, Cui P, Huang W. Highly efficient carbon utilization of coal-to-methanol process integrated with chemical looping hydrogen and air separation technology: Process modeling and parameter optimization. J Clean Prod 2020;258: 120910.

[12] Chen J, Yang S, Qian Y. A novel path for carbon-rich resource utilization with lower emission and higher efficiency: An integrated process of coal gasification and coking to methanol production. Energy 2019;177:304–18.

[13] Gräbner M, Meyer B. Performance and exergy analysis of the current developments in coal gasification technology. Fuel 2014;116:910–20.

[14] Arnaiz del Pozo C, Cloete S, Jiménez Álvaro Á. Carbon-negative hydrogen: Exploring the techno-economic potential of biomass co-gasification with CO2 capture. Energy Convers Manage 2021;247:114712.

[15] Giuffrida A, Romano M, Lozza G. Thermodynamic Assessment of IGCC Plants with Hot Gas Desulphurization. Appl Energy 2010;87(11):3374–83.

[16] Quian Zhu, "High Temperature Syngas Coolers, CCC/257" *IEA Clean Coal Centre.* 2015.

[17] Falcão DS, Pinto AMFR. A review on PEM electrolyzer modelling: Guidelines for beginners. J Clean Prod 2020;261:121184.

[18] Su C, Wei H, Wang Z, Ayed H, Mouldi A, Shayesteh AA. Economic accounting and high-tech strategy for sustainable production: A case study of methanol production from CO2 hydrogenation. Int J Hydrogen Energy 2022;47(62):25929–44.

[19] Liu Y, Li G, Chen Z, Shen Y, Zhang H, Wang S, et al. Comprehensive analysis of environmental impacts and energy consumption of biomass-to-methanol and coal-to-methanol via life cycle assessment. Energy 2020;204:117961.

[20] Trop P, Anicic B, Goricanec D. Production of methanol from a mixture of torrefied biomass and coal. Energy 2014;77:125–32.

[21] Higman C. Gasification. 2nd ed., 2008.

[22] Liu Z. Economic analysis of methanol production from coal/biomass upgrading. Energy Sources Part B 2018;13(1):66–71.

[23] Poluzzi A, Guandalini G, Guffanti S, Martinelli M, Moioli S, Huttenhuis P, et al. "Flexible Power and Biomass-To-Methanol Plants With Different Gasification Technologies" *Frontiers in Energy.* Research 2022;9.

[24] Poluzzi A, Guandalini G, Guffanti S, Elsido C, Moioli S, Huttenhuis P, et al. Flexible Power & Biomass-to-Methanol plants: Design optimization and economic viability of the electrolysis integration. Fuel 2022;310:122113.

[25] Honeywell, "Unisim Thermo Reference Guide R480 Release" 2020.

[26] Bussche KMV, Froment GF. A Steady-State Kinetic Model for Methanol Synthesis and the Water Gas Shift Reaction on a Commercial Cu/ZnO/Al2O3Catalyst. J Catal 1996;161(1):1–10.

[27] Rivera-Tinoco R, Farran M, Bouallou C, Auprêtre F, Valentin S, Millet P, et al. Investigation of power-to-methanol processes coupling electrolytic hydrogen production and catalytic CO2 reduction. Int J Hydrogen Energy 2016;41(8): 4546–59.

[28] Anantharaman R, Bolland O, Booth N, Van Dorst E, Sanchez Fernandez E, Franco F, et al. "Cesar Deliverable D2.4.3. European Best Practice Guidelines For Assessment Of Co2 Capture Technologies" 2018.

[29] Qin K, Lin W, Jensen PA, Jensen AD. High-temperature entrained flow gasification of biomass. Fuel 2012;93:589–600.

[30] A.J. Zoelle, M.J. Turner, M.C. Woods, James III PhD, Robert E, T.E. Fout and T.R. Shultz, "Cost and Performance Baseline for Fossil Energy Plants, Volume 1: Bituminous Coal and Natural Gas to Electricity, Revision 4" *Cost and Performance Baseline for Fossil Energy Plants, Volume 1: Bituminous Coal and Natural Gas to Electricity, Revision 4.* 2018.

[31] Kapetaki Z, Brandani S, Brandani P, Ahn H. Process simulation of a dual-stage Selexol process for 95% carbon capture efficiency at an integrated gasification combined cycle power plant. Int J Greenhouse Gas Control 2015;39:17–26.

[32] Mansouri Majoumerd M, De S, Assadi M, Breuhaus P. An EU initiative for future generation of IGCC power plants using hydrogen-rich syngas: Simulation results for the baseline configuration. Appl Energy 2012;99:280–90.

[33] S. Douglas, D. Breton and R. Herbanek, "Upright gasifier. Patent: WO 2009/ 020809A1" 2009.

[34] D.L. Breton, A.C. Tsang and M.W. Thompson, "Gasification system and process with staged slurry addition" 2011.

[35] Nexant I. "Preliminary feasibility analysis of RTI warm gas cleanup (WGCU). technology" 2007.

[36] D.L. Denton, "An update on RTI's warm syngas cleanup demonstration project" 2014.

[37] Dagle RA, King DL, Li XS, Xing R, Spies KA, Zhu Y, et al. Coal-Derived Warm Syngas Purification and CO2 Capture-Assisted Methane. Production 2014.

[38] Ohtsuka Y, Tsubouchi N, Kikuchi T, Hashimoto H. Recent progress in Japan on hot gas cleanup of hydrogen chloride, hydrogen sulfide and ammonia in coal-derived fuel gas. Powder Technol 2009;190(3):340–7.

[39] Kolster C, Mechleri E, Krevor S, Mac Dowell N. The role of CO2 purification and transport networks in carbon capture and storage cost reduction. Int J Greenhouse Gas Control 2017;58:127–41.

[40] T. Smolinka, E.T. Ojong and J. Garche, "Chapter 8 - Hydrogen Production from Renewable Energies—Electrolyzer Technologies" 2015, pp. 103-128.

[41] Irena. "Green hydrogen cost reduction: Scaling up electrolysers to meet the 1.5°C climate goal. International Renewable Energy Agency: Abu Dhabi" 2020.

[42] R. O'hayre, S. Cha, W. Colella and F.B. Prinz, "Fuel cell fundamentals", 2016.

[43] Ni M, Leung MK, Leung DY. Energy and exergy analysis of hydrogen production by a proton exchange membrane (PEM) electrolyzer plant. Energy Convers Manage 2008;49(10):2748–56.

[44] Thampan T, Malhotra S, Zhang J, Datta R. PEM fuel cell as a membrane reactor. Catal Today 2001;67(1–3):15–32.

[45] Biaku CY, Dale NV, Mann MD, Salehfar H, Peters AJ, Han T. A semiempirical study of the temperature dependence of the anode charge transfer coefficient of a 6 kW PEM electrolyzer. Int J Hydrogen Energy 2008;33(16):4247–54.

[46] Selamet ÖF, Acar MC, Mat MD, Kaplan Y. Effects of operating parameters on the performance of a high-pressure proton exchange membrane electrolyzer. Int J Energy Res 2013;37(5):457–67.

[47] Saeed EW, Warkozek EG. Modeling and analysis of renewable PEM fuel cell system. Energy Procedia 2015;74:87–101.

[48] N1110 Product Bulletin,"" 2016.

[49] Tijani AS, Rahim AA, Hisam MKB. A study of the loss characteristic of a high pressure electrolyzer system for hydrogen production. Jurnal Teknologi 2015;75: no. 8.

[50] Morawietz T, Handl M, Oldani C, Friedrich KA, Hiesgen R. Influence of water and temperature on ionomer in catalytic layers and membranes of fuel cells and electrolyzers evaluated by AFM. Fuel Cells 2018;18(3):239–50.

[51] Yigit T, Selamet OF. Mathematical modeling and dynamic Simulink simulation of high-pressure PEM electrolyzer system. Int J Hydrogen Energy 2016;41(32): 13901–14.

[52] Zawodzinski TA, Derouin C, Radzinski S, Sherman RJ, Smith VT, Springer TE, et al. Water uptake by and transport through Nafion® 117 membranes. J Electrochem Soc 1993;140(4):1041.

[53] Ito H, Maeda T, Nakano A, Takenaka H. Properties of Nafion membranes under PEM water electrolysis conditions. Int J Hydrogen Energy 2011;36(17):10527–40.

[54] Grigoriev SA, Kalinnikov AA, Millet P, Porembsky VI, Fateev VN. Mathematical modeling of high-pressure PEM water electrolysis. J Appl Electrochem 2010;40(5): 921–32.

[55] A.B. LaConti and L. Swette, "Special applications using PEM-technology" *Handbook of fuel cells.* 2010.

[56] Papakonstantinou G, Sundmacher K. H2 permeation through N117 and its consumption by IrOx in PEM water electrolyzers. Electrochem Commun 2019;108: 106578.

[57] Ito E, Tsukagoshi K, Masada J, Ishazaka K, Saitoh K, Torigoe T. Key technologies for ultra-high temperature gas turbines. Mitsubishi Heavy Industries Tech Rev 2015;52.

[58] Chen M, Chou S, Blaabjerg F, Davari P. Overview of Power Electronic Converter Topologies Enabling Large-Scale Hydrogen Production via Water Electrolysis. Applied Sciences 2022;12(4):1906.

[59] Upadhyay M, Lee S, Jung S, Choi Y, Moon S, Lim H. Systematic assessment of the anode flow field hydrodynamics in a new circular PEM water electrolyser. Int J Hydrogen Energy 2020;45(41):20765–75.

[60] Khan MN, Cloete S, Amini S. Efficiency Improvement of Chemical Looping Combustion Combined Cycle Power Plants. Energy Technology 2019;7(11): 1900567.

[61] Carlos Arnaiz del Pozo, Schalk Cloete, and Ángel Jiménez Álvaro. Standard Economic Assessment (SEA) Tool. Available from: https://bit.ly/3hyF1TT .

[62] Carlos Arnaiz del Pozo, Schalk Cloete and Ángel Jiménez Álvaro. SEA Tool User Guide. Available from: https://bit.ly/3jq9Bkf.

[63] SEA tool files: Methanol from solid fuels. Available from: https://bit.ly/3IJmIYg 2022.

[64] R. Turton, R.C. Bailie, W.B. Whiting and J.A. Shaeiwitz, "Analysis, synthesis and design of chemical processes", 2008.

[65] IEAGHG, L. Mancuso, N. Ferrari and J. Davison, "Capture at coal based power and hydrogen plants, Report 2014/3" 2014.

[66] Chen Q, Gu Y, Tang Z, Sun Y. Comparative environmental and economic performance of solar energy integrated methanol production systems in China. Energy Convers Manage 2019;187:63–75.

[67] R. Edwards, J. Larive, D. Rickeard and Weindorf Werner, "WELL-TO-TANK Report version 4.a: JEC WELL-TO-WHEELS ANALYSIS" *Publications Office of the European Union, JCR85326.* 2014.